Int. J. Multiphase Flow Vol. 15, No. 3, pp. 471–481, 1989
Printed in Great Britain

0301-9322/89 $3.00 + 0.00
Pergamon Press/Elsevier

PARTICLE MOTION IN A TURBULENT PIPE FLOW

A. H. GOVAN,[1] G. F. HEWITT[1] and C. F. NGAN[2]

[1]Thermal Hydraulics Division, Harwell Laboratory, Oxfordshire OX11 0RA, England

[2]Department of Chemical Engineering, Imperial College, London, England

(*Received* 1 *October* 1988; *in revised form* 15 *November* 1988)

Abstract—Experimental and numerical studies were carried out on the motion of particles in a gas stream. In the experimental part, an axial-viewing technique was used to study the motion of glass spheres of 110, 250 and 550 μm dia suspended in an air stream in a 1 m long, 32 mm dia vertical tube. The technique is different from those used in most other studies in that it gives Lagrangian measurements, in the form of velocity time-histories, from which the autocorrelation function can be calculated. In the present experiments the particle motion was found to be strongly dependent on the particle injection method. A numerical model for simulating particle motion is also described in this paper. Using this model, it was found that an axial distance of at least 300 pipe diameters is required for the particles to achieve equilibrium or long-time behaviour. It is also shown that the radial variation of the gas velocity and turbulence intensity has little effect on the particle dispersion and deposition for the reltively large particles used in this study. On the other hand, the lift force induced by the gas velocity profile gives a large reduction in deposition rate.

Key Words: pipes, turbulent flow, particle trajectories, photography, numerical simulation, deposition

1. INTRODUCTION

Flow of solid particles or liquid drops suspended in a turbulent flow in a pipe occurs in many practical situations, such as annular–mist flow in boiler tubes and pneumatic conveying of solids. For annular flow, axial-viewing techniques have been used for many years at Harwell for visualization of droplet motion. In the more recent experiments using this technique (Whalley *et al.* 1979) axial parallel beam laser illumination was employed to allow a large depth of focus. This form of the technique has been used extensively in vertical and horizontal gas–liquid flows to study the process of droplet entrainment from the liquid film in annular flow (Whalley *et al.* 1979), and the subsequent droplet motion (James *et al.* 1980; Azzopardi 1987).

Some years ago, some preliminary (and unpublished) work was done using the laser axial-viewing technique to visualize the motion of solid particles. These experiments revealed the interesting and perhaps unexpected result that, in the direction normal to the tube axis, the particles tended to travel in straight lines in spite of the effect of the turbulent fluctuations in the gas phase. In the work described in this paper this effect was examined in more detail. Experiments have been carried out with glass spheres of 110, 250 and 550 μm dia, in a 32 mm dia, 1 m long test section. High-speed ciné photography was used to record the particle motion. The experiments showed that it is possible to track such particles over many frames of the ciné films and to calculate particle velocities from them. This technique thus offers advantages over previously published methods such as LDA (e.g. Lee & Durst 1982; Wells & Stock 1983) in that time-histories of the particle motion can be obtained. Multiple flash photography (e.g. Lee *et al.* 1989) could also give time-histories but these are rather crude since the number of flashes is severely limited.

In addition, a numerical simulation of the particle motion has been carried out using a simple description of the gas flow field. The results of the experiments and the simulations indicate that for these relatively large particles the effect of the particle injection method is very persistent and "long-time" behaviour cannot be achieved in such a short tube. In view of these findings it was decided to extend the simulations to much longer tubes to determine when equilibrium or long-time behaviour is achieved. These calculations showed that the particles' r.m.s. fluctuating velocity reached a steady-state value more slowly than the mean axial velocity, the 250 μm particles requiring over 10 m of tube and a time significantly longer than the particle relaxation time.

2. EXPERIMENTAL STUDY

2.1. Experimental arrangement

The motion of 110, 250 and 550 μm glass particles (density 2600 kg/m^3) was studied using the test section shown in figure 1. The test section is of extruded acrylic tubing, 32 mm dia and 1 m length. The air enters through ports in the side-wall at the bottom of the test section and the particles are introduced through a 1.5 mm bore pipe positioned along the axis of the test section. The air flow used for the particle feed was not separately metered but was kept at the minimum necessary to maintain reliable particle flow. A total air flow of 24 kg/m^2 s was used in all the experiments described here.

The axial illumination was provided by a 5 mW He–Ne laser (wavelength 633 nm) with the beam expanded to 32 mm dia and accurately aligned with the tube axis. Another lens was used to reduce the image to a convenient size, in this case 16 mm ciné frames. The motion of the particles was recorded on high-speed ciné film (4000 frame/s) which was later analysed to give particle positions on successive ciné frames using a semi-automatic image analyser. For the 250 and 500 μm particles the entire tube cross-section was filmed but for the 110 μm particles a higher magnification was needed and therefore only one quadrant of the tube cross-section was viewed.

2.2. Particle trajectories

Figure 2 shows a typical frame from a ciné film. Particles in the focal plane of the lens (which is positioned near the top of the test section) give a sharp image, while those further down the tube appear as a series of diffraction rings. For particles near the bottom of the test section the image may become so diffuse as to be indistinguishable from the background light, particularly for small particles. An estimate of the axial position of the particle may be obtained from the following expression (Jenkins & White 1981):

$$\frac{d_i}{2z} = 1.22\frac{\lambda}{d_p}, \qquad [1]$$

where d_p is the particle diameter, λ is the wavelength of the light, d_i is the diameter of the first bright ring and z is the distance of the particle from the focal plane of the lens used to form the image. In these experiments the particle axial velocity is unknown and although it may be possible to estimate it using [1] this will not be accurate. In future experiments it may be possible to measure axial velocities using side-lighting at several axial positions.

To allow some development length for the gas and particle flow, particle positions were recorded only for particles near the top of the test section. The number of frames analysed per particle ranged from around 30 for the smallest particles, to over 200 for the largest. Some typical trajectories are shown in figure 3, together with velocities calculated from the framing rate. The trajectories are

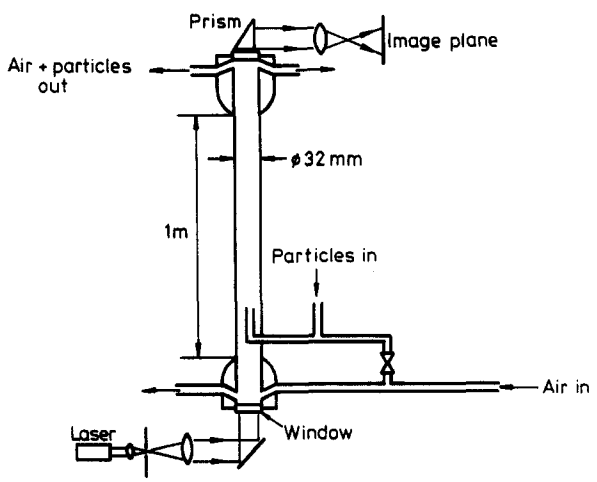

Figure 1. Axial-view experiment.

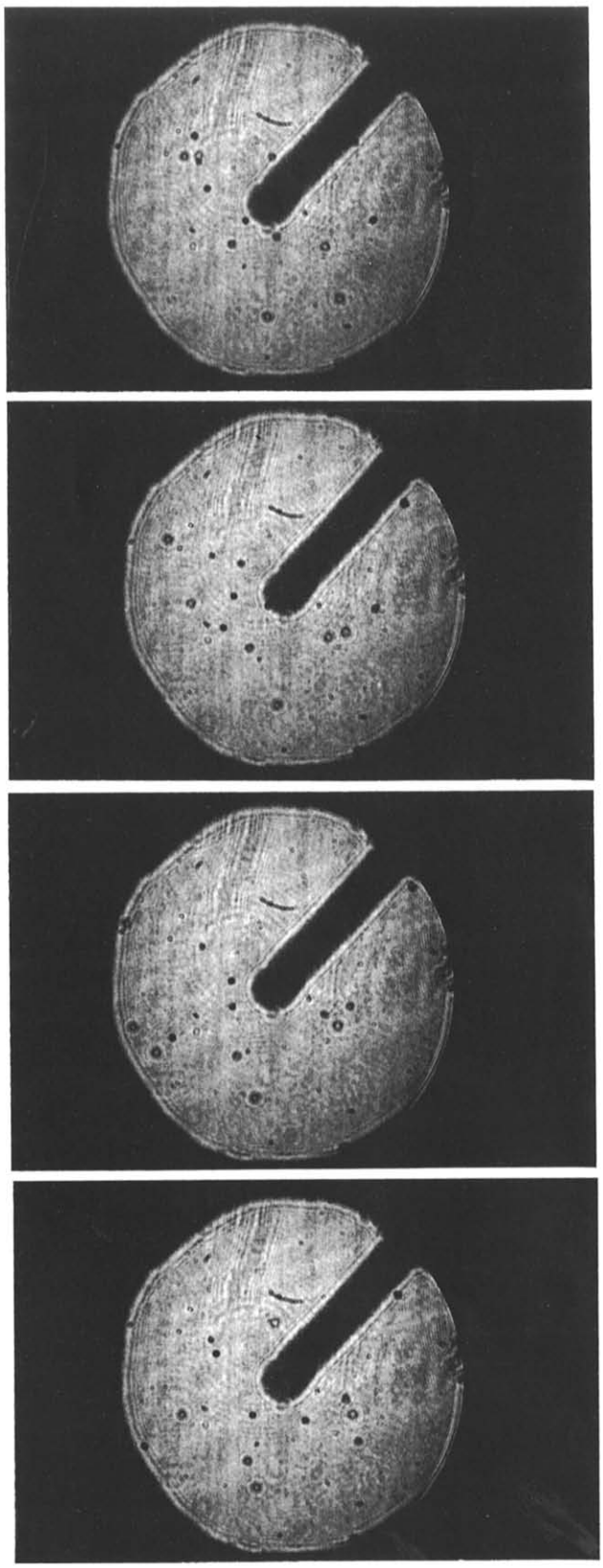

Figure 2. Sequence of frames from the ciné film showing 550 μm particles (time increment = 10 frames = 0.0025 s).

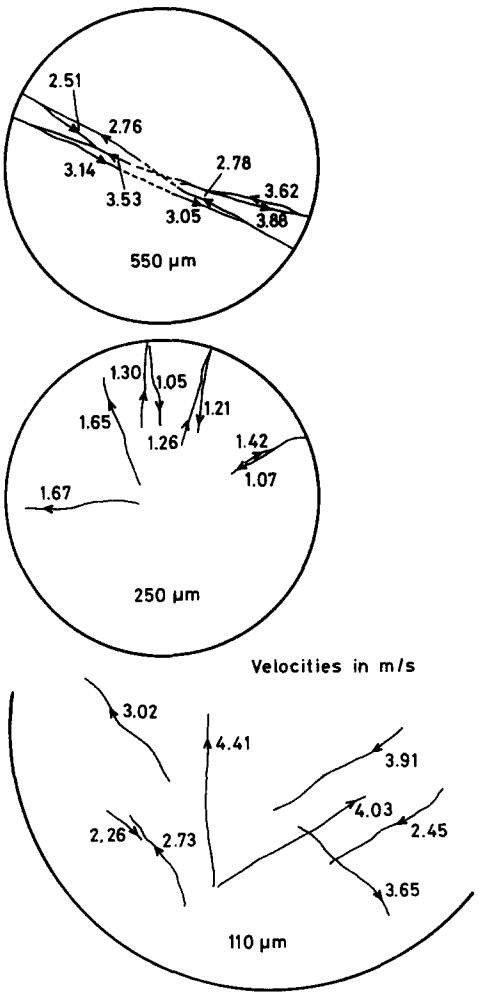

Figure 3. Measured particle trajectories.

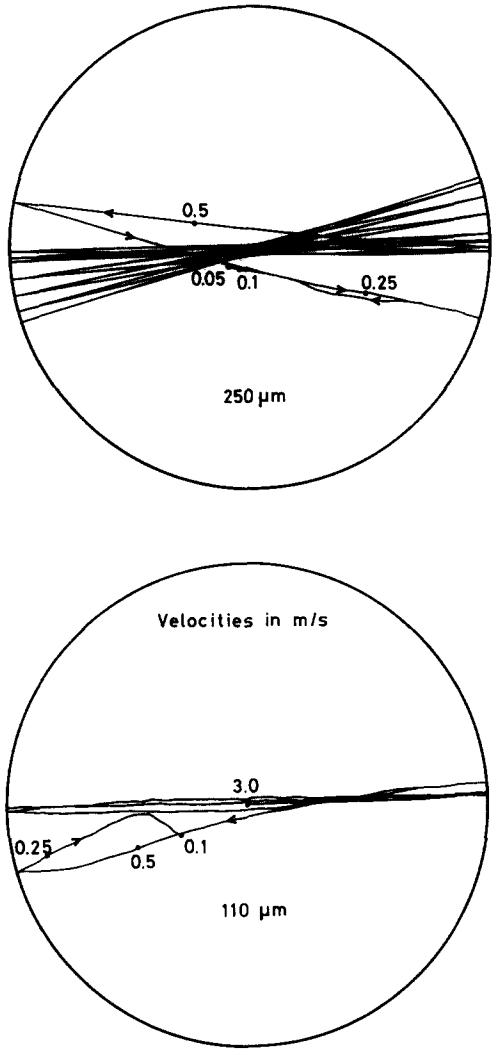

Figure 4. Simulated trajectories. $u_p(0) = 3$ m/s, $w_p(0) = 20$ m/s).

relatively straight despite the gas-phase turbulence, confirming the earlier tentative experiments. The particles were observed to frequently bounce off the walls, with mean coefficients of restitution ranging from 0.52 to 0.95.

3. NUMERICAL STUDY

3.1. Background

Although the techniques of numerical (Lagrangian) simulation are very flexible and relatively easy to apply, they have not been extensively used because they require a large amount of computing time. Nevertheless, simulation models can be very useful as research tools, for example, to check the validity of assumptions used in deriving simple analytical descriptions of particle motion. Particle motion in a turbulent flow field, such as the "core" of a pipe flow, is often treated as a diffusion process, with a long-time particle diffusion coefficient ε_p given by an expression of the form

$$\varepsilon_p = \overline{u_p^2}\tau_p, \qquad [2]$$

where $\overline{u_p^2}$ is the particle r.m.s. velocity and τ_p is the integral timescale of the particle motion, defined by

$$\tau_p = \int_0^\infty R_p(\theta)\,\mathrm{d}\theta, \qquad [3]$$

where $R_p(\theta) = \overline{u_p(t+\theta)u_p(t)}/\overline{u_p^2}$ is the Lagrangian correlation coefficient of the particle velocity.

By making simplifying assumptions is is possible to calculate ε_p. Reeks (1977), for example, assumed isotropic, homogeneous turbulence and a linear drag law. Ganic & Mastanaiah (1981), on the other hand, assumed that particle residence times were much less than τ_G, the integral timescale of the turbulence, in which case

$$\frac{\varepsilon_p}{\varepsilon_G} = \frac{\overline{u_p^2}}{\overline{u_G^2}}, \quad [4]$$

where ε_G is the gas diffusivity and $\overline{u_G^2}$ is the gas r.m.s. fluctuating velocity. Thus, ε_p can be calculated from the particles' equation of motion. In several published particle dispersion models, the results are used to predict particle deposition rates, in which case allowance must be made for the effective resistance of the laminar or quasilaminar wall-layer, since only a proportion of the particles entering this layer will have sufficient momentum to reach the wall. However, if the particles are sufficiently large that their stopping distance is greater than the thickness of this layer, then this resistance may be neglected.

In the work described in this paper the Lagrangian simulation model has been used to study particle dispersion and deposition in a turbulent pipe flow. In particular, the effect of the velocity profile and turbulence intensity profile and the induced lift forces are investigated in order to determine whether they are important in the particle dispersion and deposition processes. It is shown that for the relatively large particles used in this study the particle velocities vary only slightly with radial position and that this variation has little effect on deposition rates. On the other hand, the lift force induced by the gas velocity profile was found to give a significant reduction in the deposition rate and this should be taken into account in future work.

3.2. Basis of the model

It is assumed that the particle suspension is sufficiently dilute that one-way coupling is valid, i.e. the presence of the particles does not significantly modify the gas flow field. The gas-phase flow field is then calculated using the k–ε model of turbulence embodied in the computer program TUFC (Wilkes 1981) which gives the mean axial velocity w_G, turbulent kinetic energy k and dissipation rate ε as a function of radial position r. The calculation of particle motion is then carried out using equations similar to those given by Boysan *et al.* (1982) for cyclones. Starting from a specified initial velocity and position, the particle motion is calculated by treating it as a series of interactions with discrete eddies of characteristic size, lifetime and r.m.s. velocity given by

$$l_e = 0.3\frac{k(r)^{3/2}}{\varepsilon(r)}, \quad [5]$$

$$\tau_e = 0.12\frac{k(r)}{\varepsilon(r)} \quad [6]$$

and

$$u_e = \sqrt{\tfrac{2}{3}k(r)}. \quad [7]$$

The turbulence is assumed to be isotropic. In some cases where profile effects are not important good results can also be obtained by assuming that w_g, l_e, τ_e and u_e are independent of position and are given by (Hutchinson *et al.* 1971)

$$l_e = 0.11 d_t, \quad [8]$$

$$u_e = u^* = w_G\sqrt{\frac{f}{2}} \quad [9]$$

and

$$\tau_e = 1.6\frac{l_e}{u_e}, \quad [10]$$

where d_t is the tube diameter, u^* is the friction velocity and f is a single-phase friction factor. In [10] the factor 1.6 is the ratio of the Lagrangian and Eulerian timescales of the turbulence; there is considerable uncertainty over the actual value, reported values showing a wide range. However,

in the study described here the particles are sufficiently large that their motion is essentially Eulerian and, with the possible exception of developing particle motion, the timescale of the particle–eddy interaction is always determined by the particle–eddy "crossing" time in the vertical direction. This is consistent with the findings of previous works (e.g. Reeks 1977; Lee *et al.* 1989) that the "crossing-trajectory" effect, due to gravity, is dominant if the particle settling velocity is greater than u_e.

For each interaction, the fluctuating velocity components u', v' and w' are taken from a normal distribution with mean zero and r.m.s. u_e. Assuming the density ratio is sufficiently high that virtual mass and Basset-history forces are negligible, the equation of motion for a spherical particle is

$$m_p \frac{d\mathbf{U}_p}{dt} = C_D \tfrac{1}{2}\rho_G \frac{\pi d_p^2}{4}(\mathbf{U}_G - \mathbf{U}_p)|\mathbf{U}_G - \mathbf{U}_p|, \qquad [11]$$

where m_p is the particle mass and $\mathbf{U}_p$ and $\mathbf{U}_G$ are the particle and gas vector velocities. This was integrated to give, in a Cartesian coordinate system

$$\begin{aligned} u_p &= u'_G + (u_{p0} - u'_G)\exp(-FT), \\ v_p &= v'_G + (v_{p0} - v'_G)\exp(-FT), \\ w_p &= w_G + w'_G - \frac{g}{F} + \left(w_{p0} - w_G - w'_G + \frac{g}{F}\right)\exp(-FT); \end{aligned} \qquad [12]$$

where T is the interaction time, g is the acceleration due to gravity, u'_G, v'_G and w'_G are the fluctuating components of the instantaneous gas velocity and u_p, v_p and w_p are the components of the particle velocity, with the subscript 0 indicating the values at the start of the interaction. The parameter F, which is assumed constant during each interaction, is given by

$$F = \frac{3}{4}\frac{C_D}{d_p}\frac{\rho_G}{\rho_p}|\mathbf{U}_{p0} - \mathbf{U}_{G0}| \qquad [13]$$

with the drag coefficient given by (James *et al.* 1980):

$$C_D = \frac{24}{Re_p} + 0.44.$$

Integrating again gives the particle position (x_p, y_p, z_p),

$$\begin{aligned} x_p &= x_{p0} + u'_G T + \frac{(u_p - u'_G)[1 - \exp(-FT)]}{F} \\ y_p &= y_{p0} + v'_G T + \frac{(v_p - v'_G)[1 - \exp(-FT)]}{F} \\ z_p &= z_{p0} + \left(w_G + w'_G - \frac{g}{F}\right)T + \frac{\left(w_p - w_G - w'_G + \frac{g}{F}\right)[1 - \exp(-FT)]}{F}. \end{aligned} \qquad [14]$$

Particle position as a function of time can thus be calculated. In most of the results presented here, a coefficient of restitution of unity has been used for the particle–wall interactions, but it is a straightforward matter to replace this by a different value.

3.3. Calculated trajectories

The model described in section 3.2 has been used to calculate the behaviour of the particles in the experiments described in section 2, assuming a gas density of 1.2 kg/m^3 and a gas velocity of 20 m/s. Figures 4 and 5 show the predicted trajectories when the particles have initial radial velocities of 3 and 0 m/s, respectively. For the calculation shown in figure 5, the initial axial velocity was either 0 or 20 m/s (which may be thought of as limiting conditions). In each case the simulation was continued for 2500 interactions, corresponding to times of approx. 1.5, 3 and 10 s for the 550, 250 and 110 μm particles, respectively.

It can be seen in figure 4 that if the particles are introduced with a rather high radial velocity they travel in almost straight lines and lose momentum only very slowly. It will be shown in

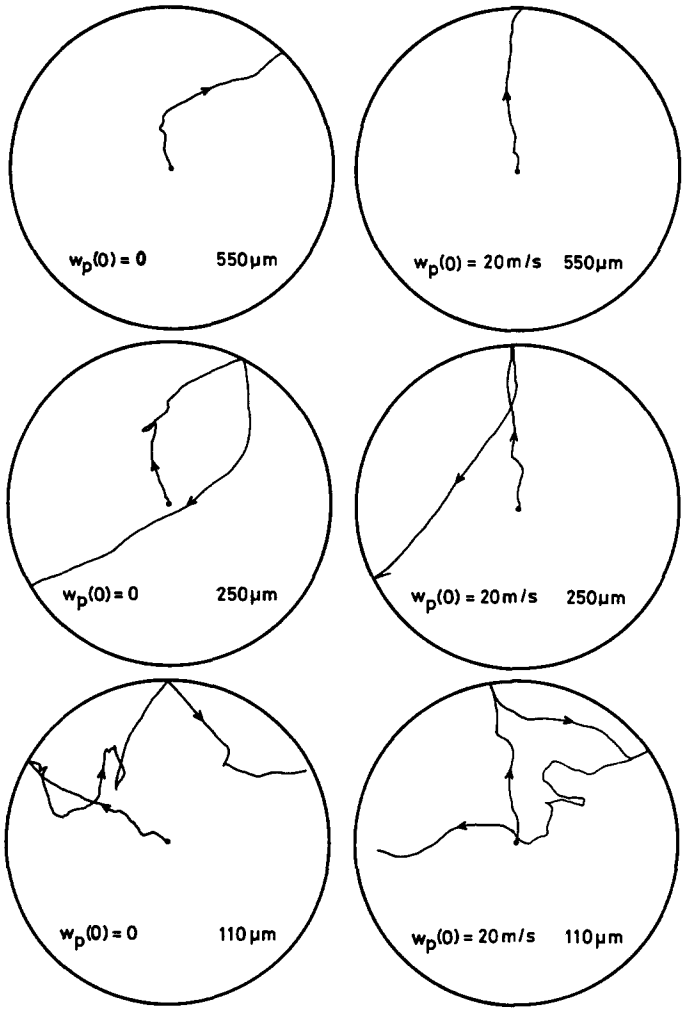

Figure 5. Simulated trajectories. $u_p(0) = 0$.

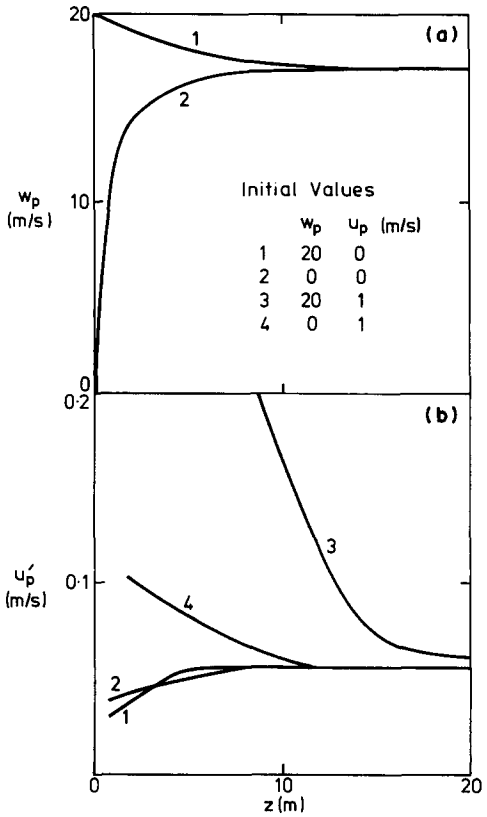

Figure 6. Development length for 250 μm particles: (a) mean axial velocity; (b) r.m.s. fluctuating velocity.

section 3.4 that the equilibrium velocity is much lower than the observed velocities in figure 3, and it is concluded that in the experiment the particles have an initial radial velocity, despite the attempt to introduce them axially. However, it can be seen from figure 5 that the larger particles travel in relatively straight lines even when they have zero initial momentum, suggesting that the integral length scale of the particle motion is comparable to, or greater than the tube diameter, or equivalently, the integral timescale of the particle motion is greater than the time taken to travel 1 tube diameter.

3.4. Fully-developed particle behaviour

Since the experiments and the simulation described in section 3.2 indicate that fully-developed, or "long-time" behaviour cannot be achieved in a 1 m long test section, the simulation model has been used to calculate the actual length of test section necessary to achieve steady-state conditions. Figure 6 shows the development length necessary for the mean and r.m.s. velocities (averaged over 200 particles) to reach steady values for the 250 μm glass particles, with various initial conditions. It can be seen that at least 10 m, and in some cases 15 m, are needed to achieve steady-state conditions. In addition, the r.m.s. velocity may take considerably longer than the mean velocity. For the 110 μm particles it was found that equilibrium conditions were achieved after about 5 m.

Figures 7 and 8 shows the time-history and autocorrelation function of the particle motion after fully-developed conditions have been achieved. This shows that the integral timescale of the particle motion is of the order of tenths of a second and is greater for the larger particles than for the smaller

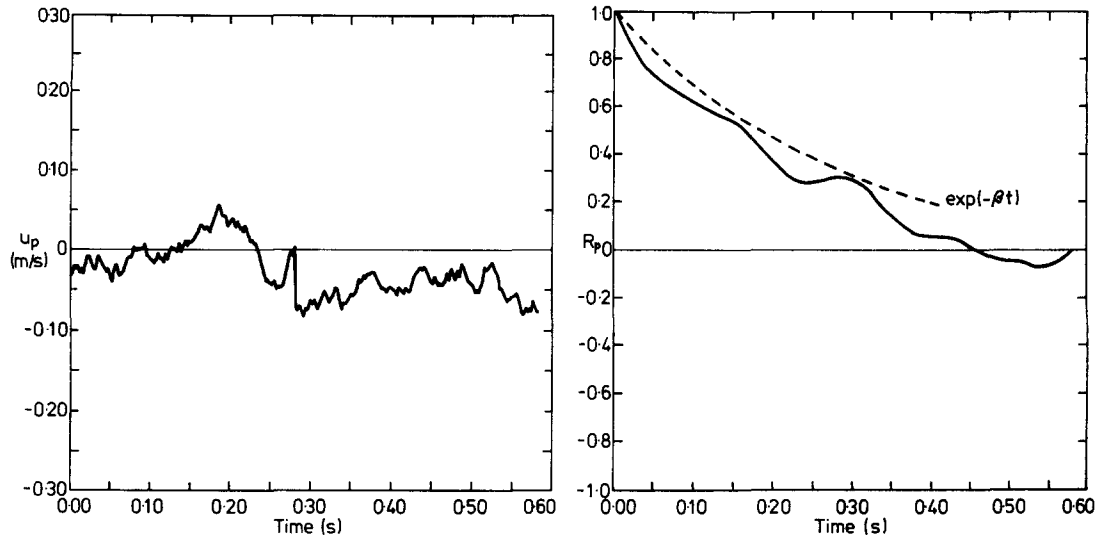

Figure 7. Time-history and autocorrelation for 250 μm particles.

ones, as expected. It can also be seen that the autocorrelation function can be reasonably well represented by an exponential, as derived by Govan (1989):

$$R_p(t) = e^{-\beta t}, \qquad [15]$$

where

$$\beta = \frac{3}{4}\frac{C_D}{d_p}\frac{\rho_G}{\rho_p}(w_G - w_p)$$

is the inverse of the particle relaxation time. For fully-developed particle motion the axial velocity w_p is approximately constant. The exponential form for the autocorrelation is consistent with the observation that the motion of large particles is a Markov process, i.e. the particle motion depends only on its present state and not on past information about the gas-phase velocity.

Thus, the integral timescale

$$\tau_p \approx \frac{1}{\beta},$$

which gives $\tau_p = 0.26$ s for the 250 μm particles.

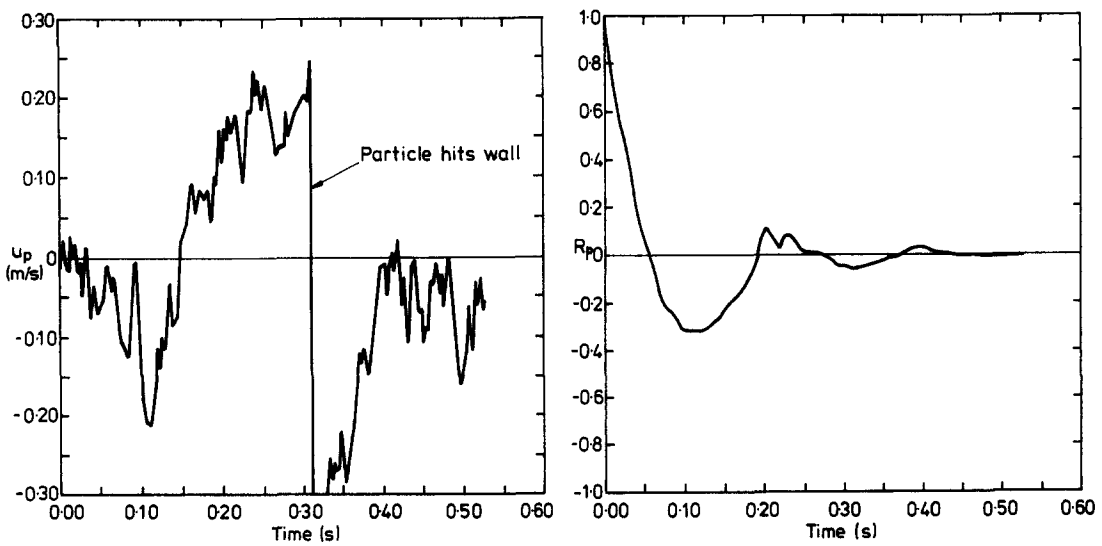

Figure 8. Time-history and autocorrelation for 110 μm particles.

3.5. *Profile effects*

In this section the simulation model has also been used to investigate the effect of the gas velocity and turbulence intensity profiles on the particle motion. This is important because it will give an indication of how well the particle dispersion can be modelled using an assumption of uniform turbulence. Figure 9 shows the mean axial and r.m.s. fluctuation velocities as a function of radial position for each particle size. Nineteen radial increments were used to obtain these plots; this required very large numbers of particles to give reasonable sample sizes in each increment. However, even with 19 increments it is likely that the behaviour close to the wall is not accurately modelled.

Figure 9 shows that the particle mean and fluctuating velocities are reasonably uniform, especially for the large particles, providing lift forces are neglected and a coefficient of restitution of unity is used. Figure 9 also shows the effect of including the lift force, calculated from the equation due to Saffman (1965):

$$m_p \frac{du_{pr}}{dt} = 6.46 \frac{d_p^2}{4} \sqrt{\rho_G \mu_G \frac{du}{dr}} (w_G - w_p), \qquad [16]$$

where m_p is the particle mass and u_{pr} is the radial component of the particle velocity. This equation was originally derived for small particle Reynolds numbers, but Hall (1988) has shown that measured lift forces on a stationary particle are predicted within a factor 2 for Reynolds numbers up to several hundred. It is recognized that this equation may not be appropriate for the particles in this study but in the absence of anything better it has been used. The inclusion of this force has a small effect on the axial particle velocity but increases the r.m.s. transverse velocity, particularly near the wall. The strong inwards acceleration due to the lift force contributes significantly to the r.m.s. velocity in this region.

Figure 9 also shows the effect of a coefficient of restitution (C.R.) much less than unity; there is a marked reduction in both axial and transverse velocities, especially close to the wall.

3.6. *Deposition rates*

Although we have been considering the motion of solid particles which rebound off the wall, the methodology used here can also be used to calculate the deposition rates of solid particles or liquid drops which adhere to the walls, a situation of obvious practical interest. For consistency with the work described in the preceding sections, the calculations have been carried out with the same particle and fluid properties as before.

Figure 10 shows the calculated deposition rate for 250 μm glass particles. The particles start on the tube axis at $z = 0$ but have a distribution of velocities equivalent to a fully-developed flow. It is clear that there is very little difference between the deposition rates calculated using the k–ε description of the flow field and those calculated using the simple description given in [8]–[10] and

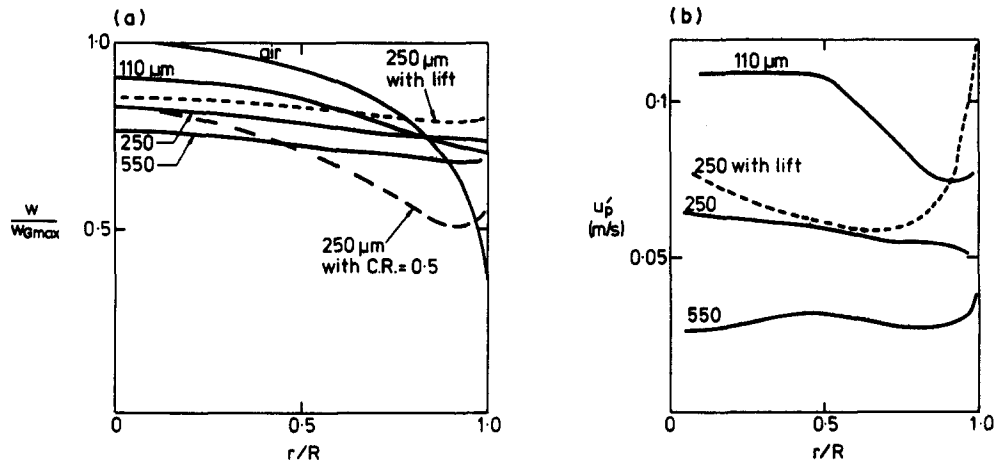

Figure 9. Profile effects: (a) mean axial velocity; (b) r.m.s. fluctuating velocity.

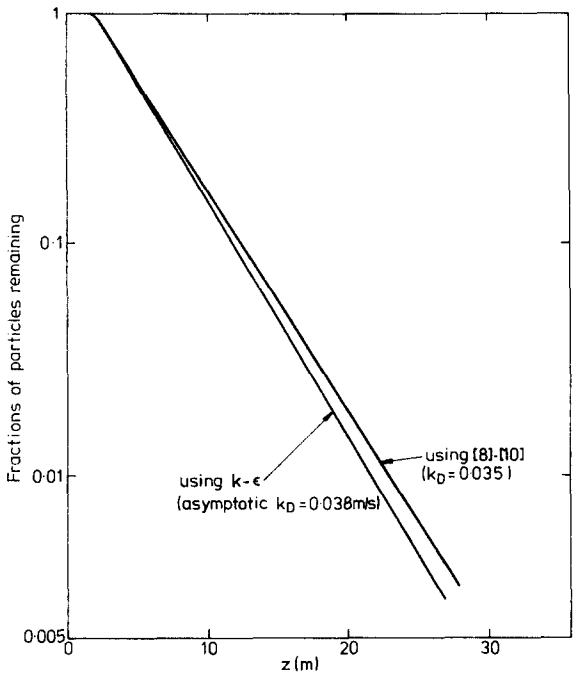

Figure 10. Particle deposition ($r = 0$ at $z = 0$).

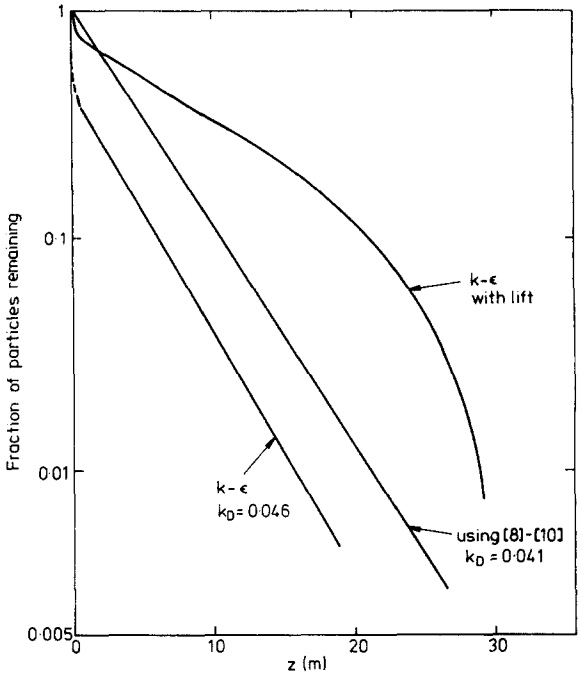

Figure 11. Particle deposition (fully-developed flow at $z = 0$).

both give straight lines on a logarithmic/linear plot, after a short development length. This implies a constant deposition coefficient

$$k_D = \frac{w_G d_t}{4(z_2 - z_1)} \ln F_1/F_2, \qquad [17]$$

where F_1 and F_2 are the fraction of particles remaining after distances z_1 and z_2. The fact that k_D is constant is surprising since the radial distribution of particles is changing with increasing axial distance.

Figure 11 shows the calculated deposition rates when $z = 0$ corresponds to a fully-developed particle flow. Again, it can be seen that the deposition coefficients are constant and are similar for the two cases with different flow descriptions of the turbulence, but in the k–ε case there is an "entrance effect" in which about 50% of the particles deposit very rapidly. Figure 11 also shows the effect of including lift forces; this results in much lower deposition rates and a significant departure from the linear deposition relation given by [17].

4. CONCLUSIONS

(i) An experimental technique has been developed for studying the motion of particles in a Lagrangian frame of reference using an axial-viewing technique. Time-histories of the motion of 110, 250 and 550 μm glass particles in a 1 m long test-section were recorded. The observed trajectories are mainly unidirectional and it is concluded that the particle motion is strongly dependent on inlet conditions.

(ii) A numerical simulation is described, which treats the particle motion as a series of interactions with discrete eddies. This model was used to study the behaviour of the particles used in the experiments. It was found that for the 250 μm particles at least 10 m of pipe are required to reach a steady-state condition. However, it was also found that in fully-developed flow the length scale of the particle motion is comparable to the tube diameter and therefore the particle motion is largely unidirectional.

(iii) The simulation model has also been used to investigate the importance of profile effects in the gas flow field in determining particle dispersion and deposition rates. It was found that the relatively large particles used in this study had much flatter mean and r.m.s. velocity profiles

than the gas-phase profiles, and as a result deposition rates can be calculated using a simple description which ignores profile effects. On the other hand, it was found that lift forces due to the gas velocity profile produce a very large reduction in deposition rates.

(iv) In future work the axial-viewing technique will be used in a 20 m long test section to study fully-developed particle motion.

Acknowledgements—This work was carried out as part of the Underlying Research Programme of the UKAEA. The authors wish to acknowledge the considerable help received from J. Terry (Photographic Group, Harwell Laboratory) in setting up and taking the axial-view ciné films.

REFERENCES

AZZOPARDI, B. J. 1987 Observations of drop motion in horizontal annular flow. *Chem. Engng Sci.* **42,** 2059–2062.

BOYSAN, F., AYERS, W. H. & SWITHENBANK, J. 1982 Cyclone design fundamentals. *Trans. Instn chem. Engrs* **60,** 4.

GANIC, E. N. & MASTANAIAH, K. 1981 Investigation of droplet deposition from a turbulent gas stream. *Int. J. Multiphase Flow* **7,** 401–422.

GOVAN, A. H. 1989 A simple equation for the diffusion coefficient of large particles in a turbulent gas flow. *Int. J. Multiphase Flow* **15,** 287–294.

HALL, D. 1988 Measurements of the mean force on a particle near a boundary in turbulent flow. *J. Fluid Mech.* **187,** 451–466.

HUTCHINSON, P., HEWITT, G. F. & DUKLER, A. E. 1971 Deposition of liquid or solid dispersions from turbulent gas streams: a stochastic model. *Chem. Engng Sci.* **26,** 419–439.

JAMES, P. W., HEWITT, G. F. & WHALLEY, P. B. 1980 Droplet motion in two-phase flow. UKAEA Report AERE-R9711.

JENKINS, F. A. & WHITE, H. E. 1981 *Fundamentals of Optics*, 4th edn, p. 329. McGraw-Hill, New York.

LEE, M. M., HANRATTY, T. J. & ADRIAN, R. J. 1989 An axial-viewing photography technique to study turbulence characteristics of particles. *Int. J. Multiphase Flow.* In press.

LEE, S. L. & DURST, F. 1982 On the motion of particles in turbulent duct flows. *Int. J. Multiphase Flow* **8,** 125–146.

REEKS, M. W. 1977 On the dispersion of small particles suspended in an isotropic turbulent fluid. *J. Fluid Mech.* **88,** 529–546.

SAFFMAN, P. W. 1965 The lift on a small sphere in a slow shear flow. *J. Fluid Mech.* **22,** 385–400; also Corrigendum **31,** 624 (1968).

WELLS, M. R. & STOCK, D. E. 1983 The effect of crossing trajectories on the dispersion of particles in a turbulent flow. *J. Fluid Mech.* **136,** 31–62.

WHALLEY, P. B., HEWITT, G. F. & TERRY, J. W. 1979 Photographic studies of two-phase flow using a parallel light technique. UKAEA Report AERE-R9389.

WILKES, N. S. 1981 Calibration of fluid flows using finite differences and the method of coordinate transformations. UKAEA Report AERE-R11218.